

BOOST-Ising: Bayesian Modeling of Spatial Transcriptomics Data via Ising Model

Xi Jiang,^{1,2} Qiwei Li,^{3, a} and Guanghua Xiao^{2, a}

¹*Department of Statistical Science, Southern Methodist University, Dallas,
TX 75275, United States*

²*Quantitative Biomedical Research Center, Department of Population and Data
Sciences, The University of Texas Southwestern Medical Center, Dallas, TX 75390,
United States*

³*Department of Mathematical Sciences, The University of Texas at Dallas,
TX 75080, United States*

Abstract

Recent technology breakthrough in spatial molecular profiling has enabled the comprehensive molecular characterizations of single cells while preserving spatial information. It provides new opportunities to delineate how cells from different origins form tissues with distinctive structures and functions. One immediate question in analysis of spatial molecular profiling data is how to identify spatially variable genes. Most of the current methods build upon the geostatistical model with a Gaussian process that relies on selecting *ad hoc* kernels to account for spatial expression patterns. To overcome this potential challenge and capture more types of spatial patterns, we introduce a Bayesian approach to identify spatially variable genes via Ising model. The key idea is to use the energy interaction parameter of the Ising model to characterize spatial expression patterns. We use auxiliary variable Markov chain Monte Carlo algorithms to sample from the posterior distribution with an intractable normalizing constant in the Ising model. Simulation results show that our energy-based modeling approach led to higher accuracy in detecting spatially variable genes than those kernel-based methods. Applying our method to two real spatial transcriptomics datasets, we discovered novel spatial patterns that shed light on the biological mechanisms. The proposed method presents a new perspective for analyzing spatial transcriptomics data.

^aTo whom correspondence should be addressed. Emails: Qiwei.Li@UTDallas.edu;

Guanghua.Xiao@UTSouthwestern.edu

I. INTRODUCTION

Cellular and molecular spatial organizations play important roles in biological functions. The development of spatial molecular profiling (SMP) techniques, which enable transcriptome measurement in high spatial resolution, has achieved significant breakthroughs in recent years (Zhang et al., 2020). Gene expression profiling approaches are no longer limited in exploring the gene expression abundance in cells via tissue-dissociation (Femino et al., 1998). SMP techniques provide new opportunities to advance our understanding of both cellular and molecular spatial organizations (Crosetto et al., 2015), and their relationships with diseases (Shah et al., 2018).

There are two major types of SMP techniques: imaging and sequencing-based. Based on the single-molecule fluorescence *in situ* hybridization (FISH), the two most famous imaging-based SMP techniques are sequential FISH (seqFISH) (Lubeck et al., 2014) and multiplexed error-robust FISH (MERFISH) (Chen et al., 2015). They can measure the expression levels of hundreds of genes on thousands of individual cells, which are irregularly scattered in a planar space. In contrast, sequencing-based techniques, such as spatial transcriptomics (ST) (Ståhl et al., 2016) and high-definition spatial transcriptomics (HDST) (Vickovic et al., 2019), use spatial barcode probes to capture RNA molecules and then synthesize and sequence their complementary DNA molecules. They can measure the expression levels of thousands of genes across hundreds of barcode probes, namely spots, each of which combines a group of cells. Those spots are usually arrayed on a two-dimensional grid.

Many new questions can be explored with emerging SMP techniques. One of the most immediate ones in analysis of SMP datasets is how to identify spatially variable (SV) genes, whose expressions exhibit spatially correlated patterns. The study of spatial patterns in gene expression could reveal significant insights into many aspects, such as embryo development (Satija et al., 2015), tumor progression (de Bruin et al., 2014), and the clinical impact of intra-tumor heterogeneity (Bedard et al., 2013). There have been several existing methods already addressing this question. Trendsceek (Edsgård et al., 2018) is based on marked point processes, and it is computationally intensive (Dries et al., 2021) and has noticeably unsatisfying performance (Sun et al., 2020). SPARK (Sun et al., 2020) and SpatialDE (Svensson et al., 2018) build upon the geostatistical model with a Gaussian process, where a kernel must be selected with caution. BinSpect (Dries et al., 2021) is an easy and fast computational method based on statistical enrichment of spatial network neighbors after binarizing gene expression levels. All the methods above can be applied to SMP data generated by both imaging and sequencing-based SMP techniques. However, none of them takes advantage of the additional spatial structure of the ST data; that is, the gene expression levels are measured on a lattice grid.

To take into account this characteristic, we develop a novel approach named Bayesian mOdeling Of Spatial Transcriptomics data via Ising model (BOOST-Ising) to identify SV genes in ST studies. BOOST-Ising comprises three steps: 1) normalizing sequence count data to relative gene expression levels; 2) dichotomizing relative gene expression levels to generate a binary spatial pattern; 3) characterizing the binary spatial pattern via inferring the Ising model interaction parameter under a Bayesian framework. The double Metropolis-Hastings

(DMH) algorithm (Liang, 2010) is used to sample from the posterior distribution with an intractable normalizing constant in the Ising model. Our approach is 1) discretization-based, which can improve the robustness to sequencing noise due to either biological or technical reasons; 2) energy-based, which is able to characterize a broader type of spatial patterns than kernel-based modeling approaches; 3) Bayesian-based, which enriches the inference via incorporating priors if necessary and naturally quantifying uncertainties. We demonstrated the advantages of BOOST-Ising on simulated data with various spatial patterns and zero-inflation settings, and also on two real ST datasets. It showed an outstanding performance compared to other alternatives.

The remainder of the paper is organized as follows. Section 2 introduces the three main components of the proposed BOOST-Ising: sequence count data normalization, relative expression level dichotomization, and binary spatial pattern characterization. In Section 3, we evaluate BOOST-Ising on simulated and two real datasets, compared with existing approaches. Section 4 concludes the article and discusses future research directions.

II. METHODS

In this section, we introduce BOOST-Ising for SV gene identification, with the schematic diagram shown in Figure 1.

Before introducing the main components, we summarize the ST data notations. Let a $n \times p$ matrix \mathbf{Y} denote the gene expression count table (i.e. molecular profile). Each entry $y_{ij} \in \mathbb{N}, i = 1, \dots, n, j = 1, \dots, p$ is the read count for gene j collected at spot i . Suppose the gene expression levels are measured on an L -by- W square lattice grid, where

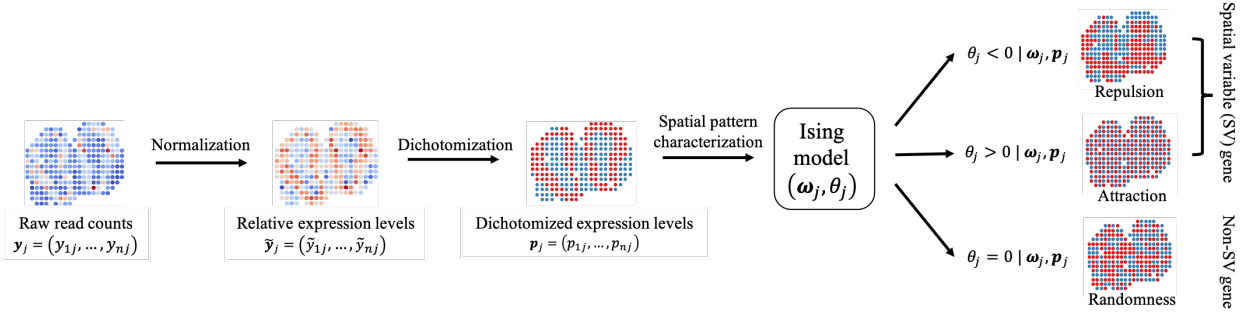


FIG. 1. The schematic diagram of BOOST-Ising

$(l, w), l = 1, \dots, L, w = 1, \dots, W$ is the coordinate of each spot. We use an $n \times 2$ matrix \mathbf{T} to represent the geospatial profile, where each row $\mathbf{t}_i \in \{1, \dots, L\} \times \{1, \dots, W\}$ indicates the spot location in the grid.

A. Normalizing sequence count data

Normalization is critical to the development of analysis techniques for any sequence count data that suffer from various sequence artifacts and bias. BOOST-Ising provides eight choices of normalization methods in two categories to counteract those biases due to biological and technical reasons.

The first type is based on size factor estimation. Let s_i be the size factor of sample i , capturing all nuisance effects. Each relative gene expression level can be computed as $\tilde{y}_{ij} = y_{ij}/s_i$. If the main interest is in the absolute gene expression level, then all s_i 's are set to the same value (e.g. $s_1 = \dots = s_n = 1$); otherwise, we compute s_i 's directly from the gene expression count data. The simplest way is to set $s_i \propto Y_i = \sum_{j=1}^p y_{ij}$, i.e., the total number of counts across all genes in each sample (known as sequencing depth or library size). Note that SPARK suggests this normalization, namely total sum scaling (TSS). In practice, we could

consider other estimations on s_i 's, which have been introduced for mitigating the influence of extremely low and high counts when analyzing bulk RNA-seq data, such as upper-quartiles (Q75) (Bullard et al., 2010), relative log expression (RLE) (Anders and Huber, 2010), and weighted trimmed mean by M-values (TMM) (Robinson and Oshlack, 2010). Table S1 in the supplement provides the definitions of the above size factor estimations. The size factor estimation is usually combined with some constraint, such as $\prod_{i=1}^n s_i = 1$.

The other type of normalization method is based on variance-stabilizing transformation (VST), which aims to transform a random variable with a negative binomial distribution into one with an approximately normal distribution. There are three options: Naïve, Anscombe (Anscombe, 1948), and logarithm, namely N-VST, A-VST, and log-VST, all of which can be abstracted as $\tilde{y}_{ij} = g(y_{ij}, \phi)$, where g is the transformation-specific function (see Table S2 in the supplement) and ϕ is the dispersion parameter estimated from the count data. Then, the relative gene expression levels are further adjusted for the log-scale total read counts, i.e. $\log Y_i$, via a linear regression model. Note that SpatialDE employs the log-VST normalization before fitting the geostatistical model.

We conducted a sensitivity analysis to evaluate BOOST-Ising under different choices of normalization methods (see Section S2 in the supplement). The graphical summary is shown in Figure S1 in the supplement. We found that 1) BOOST-Ising was considerably robust to different choices within the same category; 2) The normalization methods based on size factor estimation noticeably outperformed the VST-based methods.

B. Dichotomizing relative expression levels

After correcting for sequence artifacts and bias, we denoise the relative expression levels by partitioning all spots into two groups. This step outputs the suitable data type required in the subsequent analysis and makes BOOST-Ising more robust in the face of over-dispersion and zero-inflation, which are the two important characteristics of sequence count data.

For each gene, we introduce a binary vector $\mathbf{p}_j = (p_{1j}, \dots, p_{nj})$ to represent the dichotomization result based on its relative expression levels $(\tilde{y}_{1j}, \dots, \tilde{y}_{nj})$, with $p_{ij} = 1$ indicating gene j is highly expressed at spot i and $p_{ij} = 0$ otherwise. However, there is no consensus on the dichotomization of spots based on either absolute or relative expression level. BinSpect suggests allocating those spots with the top 30% relative expression levels to the high-expression group and the remaining to the low-expression group. Meanwhile, it also considers k -means ($k = 2$) as an alternative to avoid choosing a hard percentage rank cutoff.

BOOST-Ising provides two choices of clustering methods. The first one is similar in spirit to BinSpect- k -means, searching the \mathbf{p}_j corresponding to the minimum within-cluster sum of squares,

$$\arg \min_{\mathbf{p}_j} \sum_k \sum_i I(p_{ij} = k) (\tilde{y}_{ij} - m_k)^2,$$

where $I(\cdot)$ denotes the indicator function, $m_k = \sum_i \tilde{y}_{ij} I(p_{ij} = k) / n_k$ and $n_k = \sum_i I(p_{ij} = k)$ are the sample mean and size of each group. However, before applying k -means, BOOST-Ising first excludes those spots whose \tilde{y}_{ij} 's are larger than $\tilde{q}_j^{0.75} + 3(\tilde{q}_j^{0.75} - \tilde{q}_j^{0.25})$, where \tilde{q}_j^x is defined as the x -th sample quantile of the relative expression levels of gene j , and then

removes those spots with $y_{ij} = 0$. Note that in the context of box-and-whisker plotting, a data point is defined as an extreme outlier if it stands outside this limit. We directly allocate those discarded spots in the first and second steps to the low and high-expression groups, respectively. Compared with BinSpect, this additional preprocessing leads to a more robust performance when excessive zeros and outliers are presented in the data.

In addition to k -means that is implicitly based on pairwise distances between relative expression levels, we propose to estimate \mathbf{p}_j via fitting a two-component Gaussian mixture model (GMM) with unequal variances,

$$\tilde{y}_{ij}|p_{ij}, \boldsymbol{\mu}_j, \boldsymbol{\sigma}_j^2 \sim (1 - p_{ij})\mathcal{N}(\mu_{j0}, \sigma_{j0}^2) + p_{ij}\mathcal{N}(\mu_{j1}, \sigma_{j1}^2),$$

subjecting to $\mu_{j0} < \mu_{j1}$. Here $\boldsymbol{\mu}_j = (\mu_{j0}, \mu_{j1})$ and $\boldsymbol{\sigma}_j^2 = (\sigma_{j0}^2, \sigma_{j1}^2)$ are the group means and variances that need to be estimated. To ensure the dichotomized expression levels are of the best quality to perform the subsequent modeling, we implement the aforementioned filtering steps before fitting the GMM.

A sensitivity analysis demonstrated that BOOST-Ising performed almost equally well between the distance and model-based choices (see Section S3 and Figure S2 in the supplement).

C. Identifying SV genes via fitting an Ising model to dichotomized expression levels

Finally, we use an Ising model to quantify the spatial correlation between the two expression levels in \mathbf{p}_j across all spots \mathbf{T} under a Bayesian framework.

The Ising model, first invented by Wilhelm Lenz in 1920 (Lenz, 1920) and used in statistical mechanics, is a model of interacting binary spins on a crystalline lattice (Cipra, 1987). In our paper, spins refer to the dichotomized expression levels placed on a square lattice grid. Each non-boundary spot at $\mathbf{t}_i = (t_{i1}, t_{i2})$ is connected with four neighboring spots with the coordinates $(t_{i1} + 1, t_{i2})$, $(t_{i1} - 1, t_{i2})$, $(t_{i1}, t_{i2} + 1)$, and $(t_{i1}, t_{i2} - 1)$. For a gene of interest, each spot takes one of two values $p_{ij} = 0$ or 1. Because the spots are assigned different spins and react with their neighbors' spins, there exists a measurement of overall energy, named Hamiltonian (denoted by H),

$$H(\mathbf{p}_j | \boldsymbol{\omega}_j, \theta_j) = - \sum_i \sum_k \omega_{jk} I(p_{ij} = k) - \sum_{i \sim i'} \theta_j I(p_{ij} \neq p_{i'j}),$$

where $i \sim i'$ denotes the collection of all neighboring spot pairs. In the above equation, $\boldsymbol{\omega}_j = (\omega_{j0}, \omega_{j1})$ and θ_j represent the first and second-order intensity, where the latter is also known as the interaction parameter. We view the first term as the weighted average of the numbers of spots with different spins. The second term is proportional to the number of neighboring spot pairs with different spins. According to the Hammersley–Clifford theorem (Clifford, 1990), we can write the probability of observing a particular configuration of \mathbf{p}_j in the lattice defined by \mathbf{T} as

$$\Pr(\mathbf{p}_j | \boldsymbol{\omega}_j, \theta_j) = \frac{\exp(-H(\mathbf{p}_j | \boldsymbol{\omega}_j, \theta_j))}{\sum_{\mathbf{p}' \in \mathcal{P}} \exp(-H(\mathbf{p}' | \boldsymbol{\omega}_j, \theta_j))}, \quad (1)$$

where \mathcal{P} denotes the set of all possible configurations of spins. An exact evaluation of the normalizing constant (i.e. the denominator in the above equation) requires to sum over the entire space, which consists of 2^{LW} configurations. Taking the two real ST datasets analyzed

in the paper as examples, it needs to sum over $2^{250} \approx 1.8 \times 10^{75}$ and $2^{260} \approx 1.9 \times 10^{78}$ elements, respectively. To address this issue, we employ the double Metropolis-Hastings (DMH) algorithm (Liang, 2010) to estimate both ω_j and θ_j for each gene without calculating the normalizing constant, which are detailed in Section S1 in the supplement.

Equation (3) serves as the full data likelihood of the Bayesian Ising model. Because of the locally defined Hamiltonian energy, we can write the probability of observing each dichotomized expression level conditional on its neighboring spots' levels,

$$\Pr(p_{ij} = k|\cdot) \propto \exp\left(\omega_{jk} + \sum_{i' \in \text{Nei}(i)} \theta_j I(p_{i'j} \neq k)\right), \quad (2)$$

where $\text{Nei}(i)$ denotes the set of all neighbors to spot i . Equation (2) is essentially a logistic regression, and hence the parameters ω_j and θ_j can be interpreted in terms of conditional odds ratios in general. BOOST-Ising uses θ_j to characterize the binary spatial pattern defined by the dichotomized expression levels \mathbf{p}_j on the lattice grid \mathbf{T} . If $\theta_j = 0$, then Equation (2) reduces to $\Pr(p_{ij} = k|\cdot) = \exp(\omega_{jk}) / \sum_k \exp(\omega_{jk})$, implying that each dichotomized expression level p_{ij} is independently and identically sampled from a Bernoulli distribution with parameter $\pi_j = \exp(\omega_{j1}) / (\exp(\omega_{j0}) + \exp(\omega_{j1}))$. Thus, no spatial pattern should exhibit, and gene j is a non-SV gene. Meanwhile, ω_j characterizes the underlying abundance of low and high-expression levels in \mathbf{p}_j . Fixing the value of ω_j , Equation (2) reveals that the smaller the θ_j (i.e. $\theta_j \rightarrow -\infty$), the more likely the dichotomized expression level at any spot is concordant with the majority of its neighboring spots' levels, resulting in a repulsion pattern (i.e. the clustering of spots with the same dichotomized expression level). In contrast, when θ_j takes a large positive value, we expect an attraction pattern; that is, the

exhibition of clustering among spots with different dichotomized expression levels. Thus, the spatial correlation between the low and high-expression levels of gene j can be interpreted by θ_j . Figure 1 shows three patterns under the above three distinctive settings of θ_j conditional on $\omega_{j0} = \omega_{j1}$. It is noteworthy that those kernel-based methods, such as SPARK and SpatialDE, are only able to identify SV genes with a small subset of repulsion patterns defined by the selected kernel, while BOOST-Ising accounts for all attraction and repulsion patterns.

To complete the model specification, we impose $\theta_j \sim N(0, \sigma_\theta^2)$. As for the first-order intensity ω , we notice that an identifiability problem arises from Equation(2). For example, adding a nonzero constant c into ω_{jk} does not change the conditional probability $\Pr(p_{ij} = k | \cdot)$. Thus, we force $\omega_{j1} = 1$ and set a normal prior on $\omega_{j0} \sim N(1, \sigma_\omega^2)$.

Our primary interest lies in the identification of SV genes via making inferences on θ_j 's. We use the auxiliary variable Markov chain Monte Carlo (MCMC) algorithm, i.e. DMH, to sample from its posterior distribution. To validate if gene j exhibits a repulsion pattern, we set the null and alternative hypotheses as $\mathcal{M}_0 : \theta_j \geq 0$ and $\mathcal{M}_1 : \theta_j < 0$; while testing an attraction pattern, we set $\mathcal{M}_0 : \theta_j \leq 0$ and $\mathcal{M}_1 : \theta_j > 0$. We could select the model via calculating the Bayes factor (BF) in favor of \mathcal{M}_1 over \mathcal{M}_0 , which is defined as the ratio of posterior odds to prior odds,

$$\text{BF}_j = \frac{\Pr(\mathcal{M}_1 | \mathbf{p}_{\cdot j})}{\Pr(\mathcal{M}_0 | \mathbf{p}_{\cdot j})} \approx \frac{\Pr(\mathcal{M}_1)}{\Pr(\mathcal{M}_0)} \begin{cases} \frac{\sum_{u=1}^U I(\theta_j^{(u)} < 0) / U}{\sum_{u=1}^U I(\theta_j^{(u)} \geq 0) / U} & \text{for repulsion} \\ \frac{\sum_{u=1}^U I(\theta_j^{(u)} > 0) / U}{\sum_{u=1}^U I(\theta_j^{(u)} \leq 0) / U} & \text{for attraction} \end{cases}$$

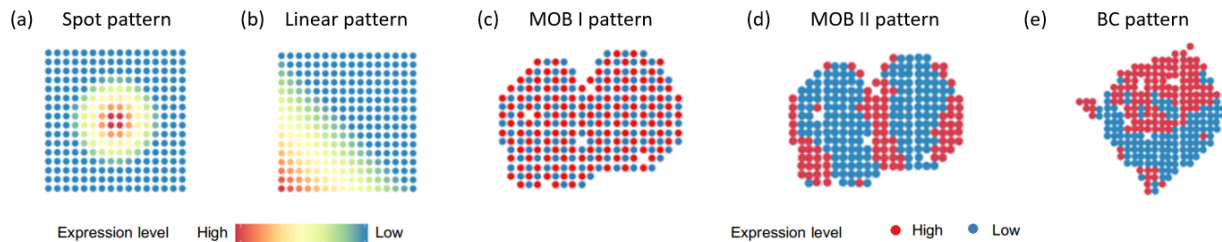


FIG. 2. Simulation study: The five spatial patterns used to generate the simulated data. (a) and (b) Two artificial patterns with the Gaussian and linear kernel; (c) An artificial pattern with complete attraction pattern, i.e. $\theta \rightarrow \infty$; (e) and (d) Two real patterns constructed from the MOB and BC study.

where the prior odds cancel out as we choose a normal prior on θ_j centered at zero, and the posterior odds can be approximated using the MCMC samples $\{\theta_j^{(1)}, \dots, \theta_j^{(U)}\}$. Here U denotes the total number of MCMC iterations after burn-in. The larger the BF_j , the more likely gene j is an SV gene, integrating over the uncertainty in all model parameters. We suggest choosing the BF threshold based on the scale for interpretation (Kass and Raftery, 1995).

III. RESULTS

A. Simulation Study

We performed a series of simulation studies to evaluate the performance of BOOST-Ising and compared it with that of three existing methods: SPARK, SpatialDE, and BinSpect. Because of the poor performance of Trendsceek reported in most literature (Dries et al., 2021; Sun et al., 2020), we did not include it here.

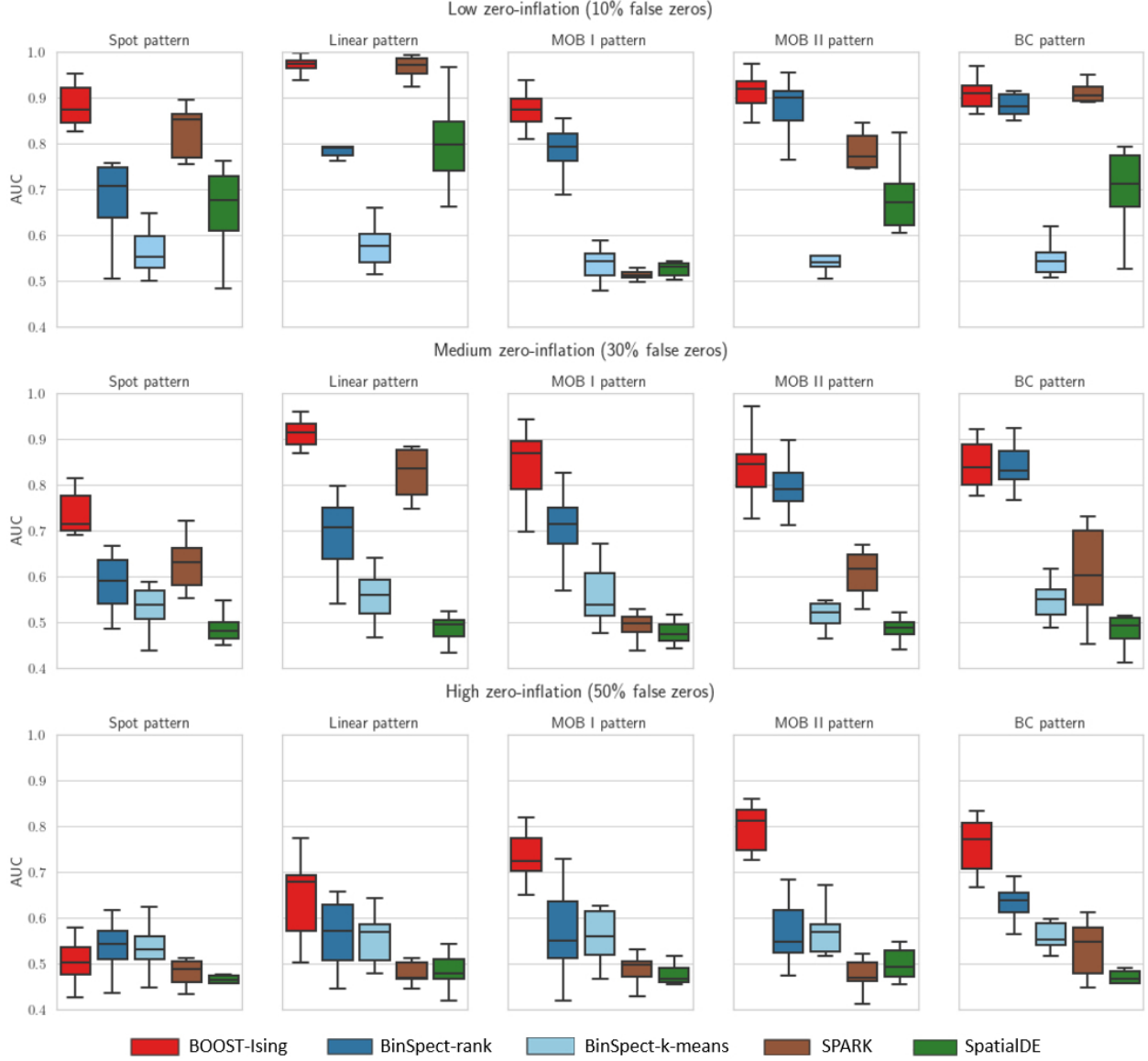


FIG. 3. Simulation study: The boxplots of AUCs achieved by BOOST-Ising, BinSpect, SPARK, and SpatialDE under different scenarios in terms of spatial pattern and zero-inflation setting.

We generated simulated data from three artificial spatial patterns (see Figure 2(a)-(c)) and two real spatial patterns (see Figure 2(d) and (e)). The two real patterns were constructed from the mouse olfactory bulb (MOB) and human breast cancer (BC) datasets analyzed in this paper. The first two artificial patterns named spot and linear were on a 16×16 square lattice ($n = 256$ spots), while the remaining one named MOB I was on

$n = 260$ spots. The MOB II and BC patterns were on $n = 260$ and 250 spots, respectively. We set $p = 100$, among which 15 were SV genes. We followed the data generative schemes (Edsgård et al., 2018; Sun et al., 2020) to simulate the gene expression count table \mathbf{Y} , which was substantially different from the model assumptions of BOOST-Ising. For each gene j , the log relative expression level at spot i was generated via,

$$\log \tilde{y}_{ij} = \begin{cases} \beta_0 + e_i + \epsilon_{ij} & \text{if gene } j \text{ is an SV gene} \\ e_i + \epsilon_{ij} & \text{otherwise} \end{cases},$$

where β_0 denotes the baseline relative expression level and ϵ_{ij} denotes the non-spatial errors following $N(0, \sigma_\epsilon^2)$. We set $\beta_0 = 2$ and $\sigma_\epsilon = 0.3$. For a non-SV gene, the relative expression levels were from a log-normal (LN) distribution with mean and variance being 2 and 0.3^2 . Consequently, no spatial correlation should be observed. For an SV gene with the spot pattern, the values of e_i 's of the four center spots at (8, 8), (8, 9), (9, 8), and (9, 9) were set to $\log 6$, while all others were linearly decreased to zero within a radius of five spots. For an SV gene with the linear pattern, the value of e_i of the most bottom-left spot at (1, 1) was set to $\log 6$, while all others were linearly decreased to zero along the diagonal line. For an SV gene with the remaining patterns, each spot was dichotomized into low and high-expression levels with $e_i = 0$ and $\log 3$, respectively. To mimic the excess zeros and over-dispersion in the real ST datasets, we sampled each gene expression count y_{ij} from a zero-inflated negative binomial (ZINB) model,

$$y_{ij} \sim \pi_i I(y_{ij} = 0) + (1 - \pi_i) \text{NB}(s_i \tilde{y}_{ij}, \phi_j),$$

where the size factor $s_i \sim \text{LN}(0, 0.2^2)$ and the dispersion parameter ϕ_j was from an exponential distribution with mean 10. For the choice of the false zero proportion π_i , we randomly selected 10%, 30%, or 50% counts and forced their values to zero. Combined with the five patterns and three zero-inflation settings, there were 15 different scenarios. For each scenario, we repeated the above steps to generate 10 replicates.

We chose to normalize the raw read counts \mathbf{Y} using TSS and dichotomize the relative expression levels for each gene using GMM as the default setting of BOOST-Ising. As for the Bayesian Ising model, the prior specification are $\omega_0 \sim \text{N}(1, \sigma_\omega^2)$ and $\theta \sim \text{N}(0, \sigma_\theta^2)$. We set $\sigma_\omega = 2.5$ and $\sigma_\theta = 1/3$. The former indicated that the underlying proportion of the low-expression spots was expected between 1% and 99% with a probability of 95% , while the latter ensured about 99% percentage of θ_j 's value ranged from -1 to 1 *a priori*. A follow-up sensitivity analysis indicated that BOOST-Ising was incredibly insensitive to the choice of these two hyperparameters (see Section S4 and Figure S3 in the supplement). As for the MCMC algorithm used to fit the Bayesian Ising model, we ran four independent MCMC chains for each gene with 10,000 iterations, discarding the first half as burn-in. We started each chain from a model by randomly drawing all parameters from their prior distributions. Results we report below were obtained by pooling together the MCMC outputs from the four chains.

BOOST-Ising identifies SV genes based on BFs, while all other competitors output p -values to guide the selection. First, we used the area under the curve (AUC) of the receiver operating characteristic (ROC) to evaluate the performance of all methods. The ROC curve was created by plotting the true positive (TP) rate against the false positive (FP) rate across

various thresholds used to select SV genes based on BFs or p -values. Second, we classified each gene to an SV or non-SV gene by pinpointing a specified threshold. Specifically, we set the BF cutoff to 150 for BOOST-Ising, corresponding to a decisive strength of evidence. To control the type-I error rate, we adjusted p -values from SPARK, SpatialDE, and BinSpect using the Benjamini-Hochberg method (Benjamini and Hochberg, 1995) and chose a significance level of 0.05 as the cutoff. We chose the Matthews correction coefficient (MCC) (Matthews, 1975),

$$\text{MCC} = \frac{(\text{TP} \times \text{TN} - \text{FP} \times \text{FN})}{\sqrt{(\text{TP} + \text{FP})(\text{TP} + \text{FN})(\text{TN} + \text{FP})(\text{TN} + \text{FN})}},$$

which balances TP, FP, true negative (TN), and false negative (FN), because SV genes were only a small subset of all genes, making other binary classification metrics not suitable. Note that AUC yields a value between 0 to 1, and MCC value ranges from -1 to 1. For both metrics, the larger the value, the more accurate the identification.

According to Figure 3, which displays the boxplots of AUCs by different methods over ten replicated datasets under each scenario, we concluded as follows. First, BOOST-Ising achieved the highest performance in terms of median AUC under 14 out of 15 scenarios, while BinSpect only had a marginal advantage over BOOST-Ising under the scenario with a high proportion of false zeros and the artificial spot pattern. Second, under the low zero-inflation setting, SPARK had a similar performance with BOOST-Ising when the SV genes were generated from linear and BC patterns. However, it suffered from reduced power under the medium and high zero-inflation settings, as did the other kernel-based method, SpatialDE. It clearly suggested that realistic modeling contributed to the advantage over SPARK. Third,

BinSpect was very sensitive to the choice of clustering methods. For example, the one based on top percentage rank performed significantly better than the one based on k -means under almost all scenarios, excluding the four scenarios with a high proportion of false zeros and the first four spatial patterns. In contrast, BOOST-Ising is considerably robust to different normalization and dichotomization methods (see Figure S1 and S2 in the supplement). Last but not least, SPARK and SpatialDE completely had no power to detect SV genes with the MOB I pattern, which was defined by a large positive interaction parameter in the Ising model. They might miss some important discoveries in real data analysis. Meanwhile, BinSpect had no satisfactory performance to detect such a pattern either, indicating our model-based analysis BOOST-Ising could sharpen inferences.

Besides, we reported the graphical and numerical summaries of all methods' performance in terms of MCCs as, shown in Figure S4 and Table S3 in the supplement, respectively. Those results led to similar conclusions.

Regarding the efficiency, the average execution time per gene was 0.004, 0.290, and 0.067 seconds for BinSpect, SPARK, and SpatialDE. BOOST-Ising spent 4.531 seconds per gene on average due to the computationally intensive MCMC algorithms, even though it was written by `Rcpp` to accelerate computation. All experiments were implemented on a high performance computing server with two Intel Xeon CPUs (45 MB cache and 2.10 GHz) and 250 GB memory.

B. Real Data Analysis

We applied BOOST-Ising to analyze two publicly available ST datasets in a mouse olfactory bulb (MOB) study and a human breast cancer (BC) study. Both of them are accessible on the Spatial Research Lab (<http://www.spatialresearch.org>). There are 12 replicates and four layers available in the MOB and BC study, respectively. Following the previous studies (Li et al., 2020; Sun et al., 2020; Svensson et al., 2018), we used the MOB replicate 11, which contains 16,218 genes measured on 262 spots, and the BC layer 2, which contains 14,789 genes measured on 251 spots. We applied the quality control steps described below. First, we excluded spots with fewer than ten total counts across all genes. Then, those genes with more than 80% zero read counts across all spots were dropped. After these two steps, the MOB data had $n = 260$ spots and $p = 9,769$ genes, while the BC data had $n = 250$ spots and $p = 2,280$ genes. We used the same prior specification, algorithm setting, and significance criteria used in the simulation study. We ran four independent MCMC chains and used the potential scale reduction factor (PSRF) (Gelman et al., 1992) to diagnose MCMC convergence. PSRF is a statistic comparing the estimated between-chains and within-chain variances for a model parameter. Its value should be close to one if multiple chains have converged to the target posterior distribution. The PSRFs for all ω_{j0} 's and θ_j 's were below 1.1, clearly suggesting that the MCMC algorithms converged. Then, for each dataset, we pooled together the outputs from the four chains and selected SV genes based on BFs. We compared BOOST-Ising with SPARK and BinSpect-rank since BinSpect with binarization based on top percentage rank consistently outperformed the one with k -means binarization

on the simulated data. Because of the poor performance of SpatialDE in our simulation study, we excluded it in real data analysis.

1. Mouse olfactory bulb (MOB) dataset

BOOST-Ising identified 734 SV genes, which was approximately the same number of SV genes detected by SPARK (772 SV genes) and around half of the number of SV genes detected by BinSpect (1,415 SV genes). Figure 4(a) is a Venn diagram showing the overlap of detected SV genes by the three methods. More than half of the SV genes identified by BOOST-Ising (388 out of 734) were also reported by both SPARK and BinSpect, while there were 221 unique SV genes to BOOST-Ising. Most of the SV genes detected by SPARK (618 out of 772) were also included in the result of BOOST-Ising or BinSpect, which indicates that SPARK is a relatively conservative method for SV gene identification. BinSpect was shown to be the most aggressive method that reported the most SV genes, more than half of which (746 out of 1,415) were not founded by either alternative.

To further explore the spatial patterns we had found, we performed the agglomerative hierarchical clustering on the SV genes identified by each of the three methods. For better visualization, we followed the data preprocessing (Sun et al., 2020; Svensson et al., 2018) to normalize the raw read counts to relative expression levels using log-VST. Next, based on the distance matrix computed from relative expression levels of all pairs of SV genes, a hierarchical clustering dendrogram was constructed. We then determined the number of clusters by cutting the hierarchical clustering dendrogram at a height corresponding to a clear separation. Last, we summarized the expression patterns via the averaged relative

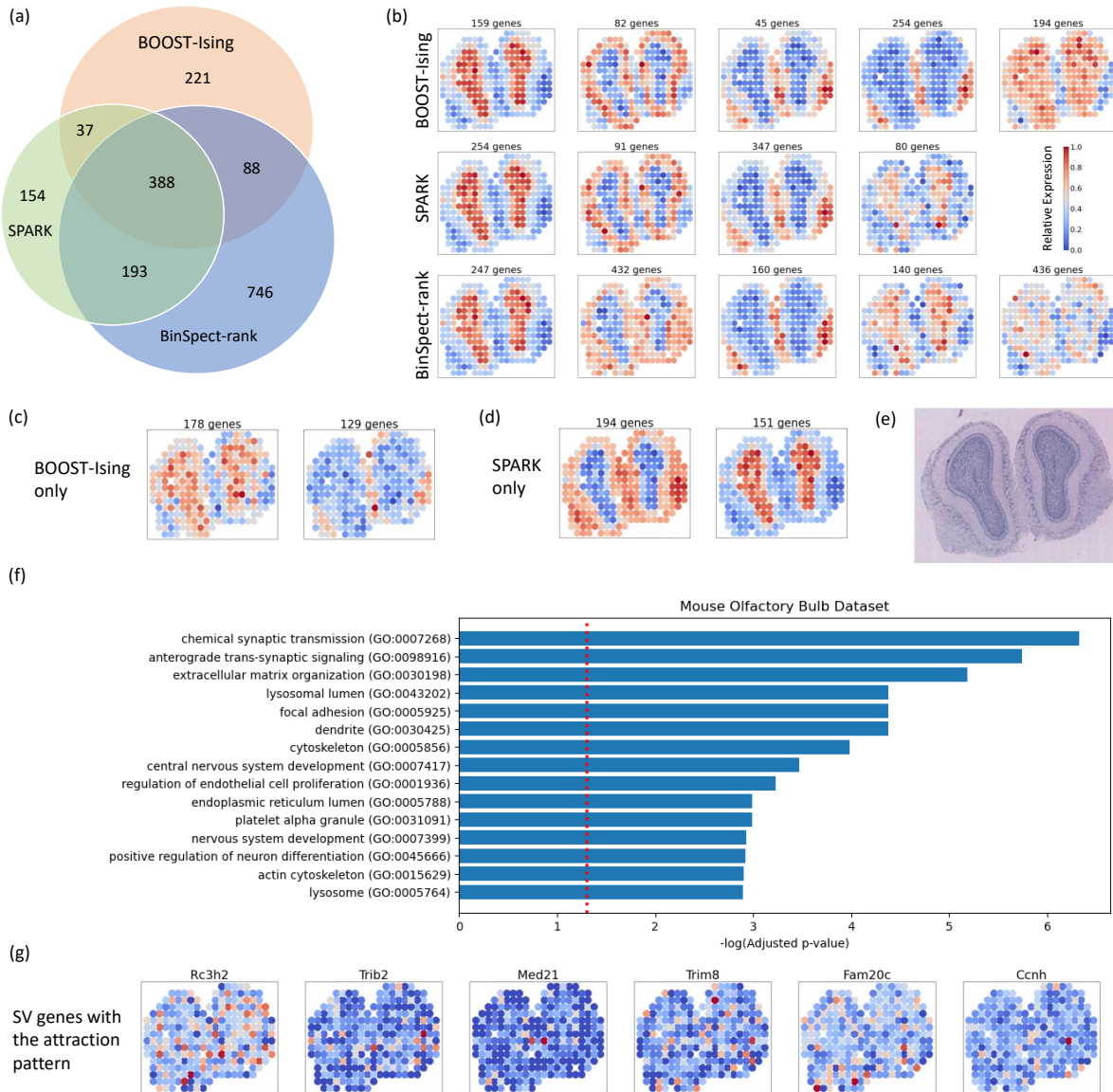


FIG. 4. Real data analysis on the MOB dataset: (a) The Venn diagram of SV genes identified by BOOST-Ising, SPARK, and BinSpect-rank; (b) Distinct spatial expression patterns summarized on the basis of 734, 772, and 1,415 SV genes identified by BOOST-Ising, SPARK, and BinSpect-rank; (c) Distinct spatial expression patterns summarized on the basis of 307 SV genes identified by BOOST-Ising only; (d) Distinct spatial expression patterns summarized on the basis of 345 SV genes identified by BOOST-Ising only; (e) The associated hematoxylin and eosin (H&E)-stained tissue slides of the analyzed MOB dataset; (f) Gene ontology (GO) enrichment analysis of 734 SV genes identified by BOOST-Ising in MOB data, with red dashed line indicating a significance level of 0.05; (g) The top six genes with the attraction pattern in terms of BF values.

expression levels within each cluster. As a result, the SV genes detected by BOOST-Ising and BinSpect were clustered into five groups, while there were four groups for SPARK, shown in Figure 4(b). Consistent with results in a previous study (Sun et al., 2020), three major spatial patterns were shown in the first three columns in Figure 4(b). Note that the fourth pattern of SPARK (with 80 genes) and BinSpect (with 140 genes) could be merged into their first pattern, respectively. Also, the third and fourth patterns of BOOST-Ising had a high similarity. It is noteworthy that a unique pattern (the last pattern of BOOST-Ising) could only be detected by BOOST-Ising with 194 SV genes, indicating our method had a higher power. To further compare BOOST-Ising with SPARK, we repeated the above procedure on those SV genes detected by BOOST-Ising or SPARK only. The results are shown in Figure 4(c) and (d), respectively. The 307 genes identified only by BOOST-Ising could be categorized into two groups, including the unique pattern with 178 genes. SV genes only detected by SPARK showed a strong periodic pattern, suggesting that SPARK might be more sensitive to the smooth periodic spatial pattern.

Next, using a Python wrapper GSEAPY (Kuleshov et al., 2016; Subramanian et al., 2007), we performed gene ontology (GO) enrichment analysis of the 734 SV genes identified by BOOST-Ising to explore their relevant biological functions. A total of 3,929 mouse GO terms in three components (biological processes, cellular components, and molecular functions) had at least one gene overlap. Controlling the false discovery rate (FDR) at 5%, we found 155 GO terms, the top 15 of which (with the smallest p -values) are shown in Figure 4(f). As with SPARK, many enriched gene sets were related to synaptic signaling and the nervous system, both of which are significantly associated with the synaptic organization

and olfactory bulb development (Treloar et al., 2010). Examples include chemical synaptic transmission (GO:0007268; adjusted p -value 4.69×10^{-7}) and nervous system development (GO:0007399; adjusted p -value 1.18×10^{-3}).

Last but not least, BOOST-Ising identified 60 genes that had an attraction pattern with a positive interaction parameter in the Ising model. Table S4 in the supplement lists all of them. To analyze the potential biological functions of these SV genes, we performed functional enrichment analysis. There were 603 mouse GO terms and 43 Kyoto Encyclopedia of Genes and Genomes (KEGG) terms with at least one gene overlapping with those SV genes. We also found some statistically significant GO and KEGG terms, which had adjusted p -values less than a significance level of 0.05. For example, holo TFIID complex (GO:0005675) and nucleotide excision repair KEGG term were significantly enriched (adjusted p -value 0.040 and 0.013, respectively). In all, these discoveries highlighted the advantage of implementing gene spatial expression analysis with BOOST-Ising.

2. Human breast cancer (BC) dataset

There were 302 SV genes identified by BOOST-Ising, which was slightly larger than the number of SV genes detected by SPARK (292 SV genes) and around one-tenth of the number of SV genes detected by BinSpect (3,278 SV genes). A Venn diagram, as shown in Figure 5(a), indicates that over 40% of the SV genes detected by BOOST-Ising (124 out of 302) were in common with the result obtained by both SPARK and BinSpect. There were only 27 SV genes identified only by BOOST-Ising. Once again, it demonstrated that SPARK is a conservative method and Binspect is an aggressive one, since nearly 90% of the SV genes

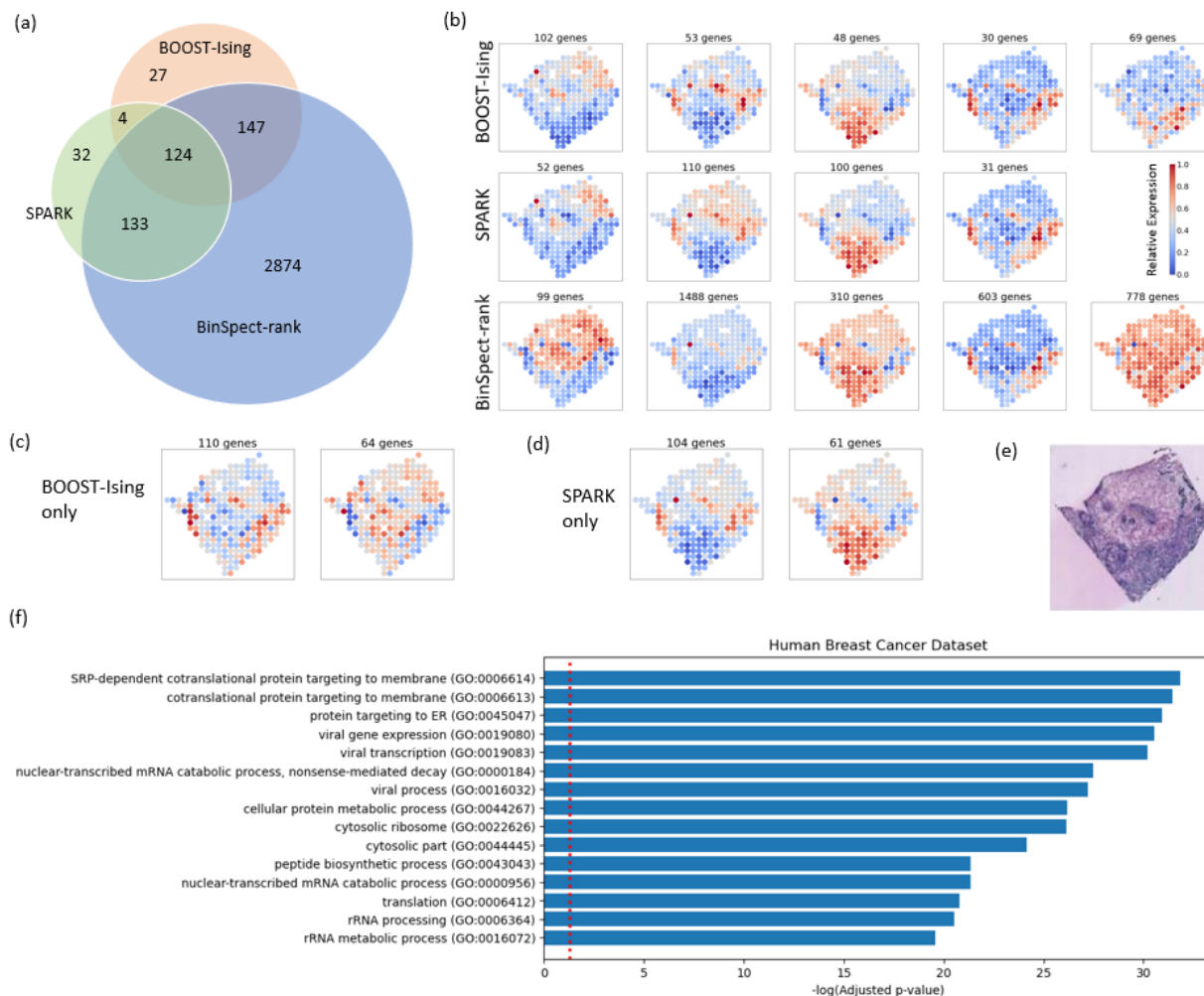


FIG. 5. Real data analysis on the BC dataset: (a) The Venn diagram of SV genes identified by BOOST-Ising, SPARK, and BinSpect-rank; (b) Distinct spatial expression patterns summarized on the basis of 302, 292, and 3,278 SV genes identified by BOOST-Ising, SPARK, and BinSpect-rank; (c) Distinct spatial expression patterns summarized on the basis of 174 SV genes identified by BOOST-Ising only; (d) Distinct spatial expression patterns summarized on the basis of 165 SV genes identified by BOOST-Ising only; (e) The associated hematoxylin and eosin (H&E)-stained tissue slides of the analyzed BC dataset; (f) Gene ontology (GO) enrichment analysis of 302 SV genes identified by BOOST-Ising in MOB data, with red dashed line indicating a significance level of 0.05.

detected by SPARK (260 out of 292) were also included in the results of BOOST-Ising or BinSpect, while nearly 90% of the SV genes reported by BinSpect (2,874 out of 3,278) were found by neither BOOST-Ising nor BinSpect.

We reported more detailed analysis results, following the same procedure when studying the MOB dataset. Each row in Figure 5(b) shows the distinct expression patterns detected by BOOST-Ising, SPARK, and BinSpect, respectively. There were five, four, and five groups obtained by performing the agglomerative hierarchical clustering. It is noteworthy that BOOST-Ising successfully detected all four patterns discovered by SPARK. However, BOOST-Ising detected 102 SV genes with the first pattern, while SPARK reported only 52 SV genes with a similar pattern. BOOST-Ising identified fewer SV genes than SPARK for the second and third patterns, while the number of SV genes was almost the same for the fourth pattern. The last pattern of BOOST-Ising was unique, and it was approximately the reversed pattern of the first one. Additionally, we did the same clustering procedure on the SV genes only detected by BOOST-Ising and SPARK, which is shown in Figure 5(c) and (d). In this BC study, BOOST-Ising reported no SV genes with an attraction pattern.

Finally, we performed GO enrichment analysis of the 302 SV genes identified by BOOST-Ising. A total of 2,477 human GO terms had at least one gene overlap with those identified SV genes. At an FDR of 5%, 116 GO terms were found. Figure 5(f) shows the top 15 GO terms with the smallest adjusted p -values. SPARK discovered many enriched gene sets, which were related to extracellular matrix organization and immune responses (Sun et al., 2020). Although these GO terms were not shown in Figure 5(f), BOOST-Ising did detect the same related terms with a significant result (e.g. the adjusted p -value for extracellular

matrix organization (GO:0030198) was 1.53×10^{-14}). Furthermore, more virus-related GO terms were found to be significant in our analysis. There is strong evidence that many types of the virus may have a causal relationship with human breast cancers (Lawson and Heng, 2010). For example, virus life cycle GO term (GO:0019058) was significantly enriched in the reported SV genes by BOOST-Ising, while not statistically significant for SV genes identified by SPARK (the adjusted p -value was only 0.829).

IV. CONCLUSION

In this paper, we develop BOOST-Ising to analyze ST data based on the Ising model. Instead of characterizing an SV gene via a pre-specified kernel by most existing methods, we define a spatial pattern via the Hamiltonian energy in the Ising model. BOOST-Ising offers the flexibility to choose different normalization and dichotomization methods, and it is considerably robust to biological and technique noise and bias. In the simulation study, BOOST-Ising had a noticeable advantage over alternative methods, especially when there were a great number of zeros in the data. This is very encouraging since BOOST-Ising does not directly model excess zeros. BOOST-Ising led to more discoveries in real data analysis, such as novel spatial patterns that had never been reported and novel SV genes that kernel-based methods are unable to detect.

Several extensions of our model are worth investigating. First of all, the proposed model could be extended to model k discrete gene expression levels via a Potts model or its modified version to characterize finer spatial patterns. The number of components k can even be estimated (Green and Richardson, 2002). Second, based on the multi-stage BOOST-Ising,

a full hierarchical Bayesian framework could be developed to directly model the ST count data to sharpen inference. For example, with a joint Bayesian inference, BOOST-Ising could further incorporate pathway information as prior knowledge to integrate the regulatory relationships between genes to perform a joint selection on SV genes. Moreover, since our approach requires the gene expression measured on a lattice grid, it is necessary to generalize our model to detect SV genes from SMP data produced by other platforms, such as seqFISH and MERFISH. Finally, it is possible to investigate other approximate Bayesian computation methods to reduce the computational cost of BOOST-Ising. These future directions could potentially further improve the performance of BOOST-Ising.

DATA AVAILABILITY

Two publicly available ST datasets in a mouse olfactory bulb study and a human breast cancer study are accessible on the Spatial Research Lab (<http://www.spatialresearch.org>). All simulated and real data used for analysis, and the related source code in R/C++ are available at <https://github.com/Xijiang1997/BOOST-Ising>.

ACKNOWLEDGEMENTS

Computational support was generously provided by Southern Methodist University’s Center for Research Computing. The authors would like to thank Suhana Bedi from the University of Texas at Dallas for helping us summarizing and implementing the normalization methods, and Jessie Norris from the University of Texas Southwestern Medical Center for helping us in proofreading the manuscript.

FUNDING

This study was partially supported by the National Institutes of Health (NIH) [1R01GM140012, P30CA142543] and the Cancer Prevention and Research Institute of Texas [RP190107]. The funders had no role in the design of the study and collection, analysis, and interpretation of data and in writing the manuscript.

REFERENCES

- Anders, S. and W. Huber (2010). Differential expression analysis for sequence count data. *Nature Precedings*, 1–1.
- Anscombe, F. J. (1948). The transformation of Poisson, binomial and negative-binomial data. *Biometrika* 35(3/4), 246–254.
- Bedard, P. L., A. R. Hansen, M. J. Ratain, and L. L. Siu (2013). Tumour heterogeneity in the clinic. *Nature* 501(7467), 355–364.
- Benjamini, Y. and Y. Hochberg (1995). Controlling the false discovery rate: A practical and powerful approach to multiple testing. *Journal of the Royal Statistical Society: Series B (Methodological)* 57(1), 289–300.
- Bullard, J. H., E. Purdom, K. D. Hansen, and S. Dudoit (2010). Evaluation of statistical methods for normalization and differential expression in mRNA-seq experiments. *BMC Bioinformatics* 11(1), 1–13.
- Chen, K. H., A. N. Boettiger, J. R. Moffitt, S. Wang, and X. Zhuang (2015). Spatially resolved, highly multiplexed RNA profiling in single cells. *Science* 348(6233).
- Cipra, B. A. (1987). An introduction to the Ising model. *The American Mathematical Monthly* 94(10), 937–959.
- Clifford, P. (1990). Markov random fields in statistics. *Disorder in physical systems: A volume in honour of John M. Hammersley*, 19–32.

- Crosetto, N., M. Bienko, and A. Van Oudenaarden (2015). Spatially resolved transcriptomics and beyond. *Nature Reviews Genetics* 16(1), 57–66.
- de Bruin, E. C., N. McGranahan, R. Mitter, M. Salm, D. C. Wedge, L. Yates, M. Jamal-Hanjani, S. Shafi, N. Murugaesu, A. J. Rowan, et al. (2014). Spatial and temporal diversity in genomic instability processes defines lung cancer evolution. *Science* 346(6206), 251–256.
- Dries, R., Q. Zhu, R. Dong, C.-H. L. Eng, H. Li, K. Liu, Y. Fu, T. Zhao, A. Sarkar, F. Bao, et al. (2021). Giotto: A toolbox for integrative analysis and visualization of spatial expression data. *Genome Biology* 22(1), 1–31.
- Edsgård, D., P. Johnsson, and R. Sandberg (2018). Identification of spatial expression trends in single-cell gene expression data. *Nature Methods* 15(5), 339–342.
- Femino, A. M., F. S. Fay, K. Fogarty, and R. H. Singer (1998). Visualization of single RNA transcripts in situ. *Science* 280(5363), 585–590.
- Gelman, A., D. B. Rubin, et al. (1992). Inference from iterative simulation using multiple sequences. *Statistical Science* 7(4), 457–472.
- Green, P. J. and S. Richardson (2002). Hidden Markov models and disease mapping. *Journal of the American Statistical Association* 97(460), 1055–1070.
- Kass, R. E. and A. E. Raftery (1995). Bayes factors. *Journal of the American Statistical Association* 90(430), 773–795.
- Kuleshov, M. V., M. R. Jones, A. D. Rouillard, N. F. Fernandez, Q. Duan, Z. Wang, S. Koplev, S. L. Jenkins, K. M. Jagodnik, A. Lachmann, et al. (2016). Enrichr: A comprehensive gene set enrichment analysis web server 2016 update. *Nucleic Acids Research* 44(W1), W90–W97.

- Lawson, J. S. and B. Heng (2010). Viruses and breast cancer. *Cancers* 2(2), 752–772.
- Lenz, W. (1920). Contribution v s ge to the v s understanding of the magnetic properties in solid bodies. *Physical Z* 21, 613–615.
- Li, Q., M. Zhang, Y. Xie, and G. Xiao (2020). Bayesian modeling of spatial molecular profiling data via Gaussian process. *arXiv preprint arXiv:2012.03326*.
- Liang, F. (2010). A double Metropolis-Hastings sampler for spatial models with intractable normalizing constants. *Journal of Statistical Computation and Simulation* 80(9), 1007–1022.
- Love, M. I., W. Huber, and S. Anders (2014). Moderated estimation of fold change and dispersion for RNA-seq data with deseq2. *Genome Biology* 15(12), 1–21.
- Lubeck, E., A. F. Coskun, T. Zhiyentayev, M. Ahmad, and L. Cai (2014). Single-cell in situ RNA profiling by sequential hybridization. *Nature Methods* 11(4), 360.
- Matthews, B. W. (1975). Comparison of the predicted and observed secondary structure of T4 phage lysozyme. *Biochimica et Biophysica Acta (BBA)-Protein Structure* 405(2), 442–451.
- Robinson, M. D. and A. Oshlack (2010). A scaling normalization method for differential expression analysis of RNA-seq data. *Genome Biology* 11(3), 1–9.
- Satiya, R., J. A. Farrell, D. Gennert, A. F. Schier, and A. Regev (2015). Spatial reconstruction of single-cell gene expression data. *Nature Biotechnology* 33(5), 495–502.
- Shah, S., Y. Takei, W. Zhou, E. Lubeck, J. Yun, C.-H. L. Eng, N. Koulena, C. Cronin, C. Karp, E. J. Liaw, et al. (2018). Dynamics and spatial genomics of the nascent transcriptome by intron seqFISH. *Cell* 174(2), 363–376.

- Ståhl, P. L., F. Salmén, S. Vickovic, A. Lundmark, J. F. Navarro, J. Magnusson, S. Giacomello, M. Asp, J. O. Westholm, M. Huss, et al. (2016). Visualization and analysis of gene expression in tissue sections by spatial transcriptomics. *Science* 353(6294), 78–82.
- Subramanian, A., H. Kuehn, J. Gould, P. Tamayo, and J. P. Mesirov (2007). Gsea-p: A desktop application for gene set enrichment analysis. *Bioinformatics* 23(23), 3251–3253.
- Sun, S., J. Zhu, and X. Zhou (2020). Statistical analysis of spatial expression patterns for spatially resolved transcriptomic studies. *Nature Methods* 17(2), 193–200.
- Svensson, V., S. A. Teichmann, and O. Stegle (2018). SpatialDE: Identification of spatially variable genes. *Nature Methods* 15(5), 343–346.
- Treloar, H. B., A. M. Miller, A. Ray, and C. A. Greer (2010). Development of the olfactory system. *The Neurobiology of Olfaction* 20092457, 131–155.
- Vickovic, S., G. Eraslan, F. Salmén, J. Klughammer, L. Stenbeck, D. Schapiro, T. Äijö, R. Bonneau, L. Bergenstråhle, J. F. Navarro, et al. (2019). High-definition spatial transcriptomics for in situ tissue profiling. *Nature Methods* 16(10), 987–990.
- Zhang, M., T. Sheffield, X. Zhan, Q. Li, D. M. Yang, Y. Wang, S. Wang, Y. Xie, T. Wang, and G. Xiao (2020). Spatial molecular profiling: Platforms, applications and analysis tools. *Briefings in Bioinformatics*.

SUPPLEMENTARY NOTES

S1. DETAILS OF DOUBLE METROPOLIS-HASTINGS (DMH) ALGORITHMS

As described in the Methods section, the binary expression indicator \mathbf{p}_j is modeled via an Ising model (Cipra, 1987), which has the probability mass function:

$$\Pr(\mathbf{p}_j|\boldsymbol{\omega}_j, \theta_j) = \frac{\exp(-H(\mathbf{p}_j|\boldsymbol{\omega}_j, \theta_j))}{\sum_{\mathbf{p}' \in \mathcal{P}} \exp(-H(\mathbf{p}'|\boldsymbol{\omega}_j, \theta_j))},$$

where the Hamiltonian H is defined as

$$H(\mathbf{p}_j|\boldsymbol{\omega}_j, \theta_j) = - \sum_i \sum_k \omega_{jk} I(p_{ij} = k) - \sum_{i \sim i'} \theta_j I(p_{ij} \neq p_{i'j}).$$

To avoid calculating the intractable normalizing constant $C(\boldsymbol{\omega}_j, \theta_j) = \sum_{\mathbf{p}' \in \mathcal{P}} \exp(-H(\mathbf{p}'|\boldsymbol{\omega}_j, \theta_j))$, we employ the double Metropolis-Hastings (DMH) algorithm (Liang, 2010) to estimate both $\boldsymbol{\omega}_j$ and θ_j for each gene. The full data likelihood can be written as

$$f(\mathbf{p}_j|\boldsymbol{\omega}_j, \theta_j) = \frac{1}{C(\boldsymbol{\omega}_j, \theta_j)} \exp \left(\sum_i \sum_k \omega_{jk} I(p_{ij} = k) + \sum_{i \sim i'} \theta_j I(p_{ij} \neq p_{i'j}) \right). \quad (3)$$

The model parameter space consists of $(\theta_j, \boldsymbol{\omega}_j)$, where θ_j is the interaction parameter between the low and high-expression states and $\boldsymbol{\omega}_j = (\omega_{j0}, \omega_{j1})$ are the first-order intensity parameters of the low and high-expression levels. We place a normal prior distribution on θ_j :

$$\pi(\theta_j) = \text{N}(\theta_j; 0, \sigma_\theta^2) \propto \exp \left(-\frac{\theta_j^2}{2\sigma_\theta^2} \right).$$

For first-order intensity parameter $\boldsymbol{\omega}_j = (\omega_{j0}, \omega_{j1})$, we fix $\omega_{j1} = 1$ to avoid the identifiability problem and only estimate ω_{j0} . We assign a normal prior distribution on ω_{j0} :

$$\pi(\omega_{j0}) = \text{N}(\omega_{j0}; 1, \sigma_\omega^2) \propto \exp\left(-\frac{(\omega_{j0} - 1)^2}{2\sigma_\omega^2}\right).$$

Thus, the full posterior is

$$\pi(\omega_{j0}, \theta_j | \mathbf{p}_j) \propto f(\mathbf{p}_j | \omega_{j0}, \theta_j) \pi(\omega_{j0}) \pi(\theta_j),$$

where $f(\mathbf{p}_j | \omega_{j0}, \theta_j) = f(\mathbf{p}_j | \boldsymbol{\omega}_j, \theta_j)$ with $\boldsymbol{\omega}_j = (\omega_{j0}, 1)$, according to Equation (3).

Update of interaction parameter θ_j : To avoid calculating intractable normalizing constant, we use the DMH algorithm (Liang, 2010) to update θ_j . Specifically, we first simulate a new sample θ'_j from $\pi(\theta_j)$ using the MH algorithm starting with θ_j . Then, we generate an auxiliary variable \mathbf{p}'_j through m MH updates starting with the current state \mathbf{p}_j based on the new value θ'_j and accept it with probability $\min(1, R_{\theta_j})$, where,

$$R_{\theta_j} = \frac{f(\mathbf{p}'_j | \boldsymbol{\omega}_j, \theta_j) f(\mathbf{p}_j | \boldsymbol{\omega}_j, \theta'_j) \pi(\theta'_j)}{f(\mathbf{p}_j | \boldsymbol{\omega}_j, \theta_j) f(\mathbf{p}'_j | \boldsymbol{\omega}_j, \theta'_j) \pi(\theta_j)}$$

If auxiliary variable \mathbf{p}'_j is accepted, update θ_j to θ'_j . Otherwise, set θ_j to the current value.

Update of first-order intensity parameter ω_{j0} : Same as updating θ_j , we use the DMH algorithm (Liang, 2010) to update ω_{j0} . Specifically, we first simulate a new sample $\omega'_{j0} = (\omega'_{j0}, 1)$ from $\pi(\omega_{j0})$ using the MH algorithm starting with ω_{j0} . Then, we generate an auxiliary variable \mathbf{p}'_j through m MH updates starting with the current state \mathbf{p}_j based on the

new value ω'_j and accept it with probability $\min(1, R_{\omega_j})$, where,

$$R_{\omega_j} = \frac{f(\mathbf{p}'_j|\omega_j, \theta_j)f(\mathbf{p}_j|\omega'_j, \theta_j) \pi(\omega'_{j0})}{f(\mathbf{p}_j|\omega_j, \theta_j)f(\mathbf{p}'_j|\omega'_j, \theta_j) \pi(\omega_{j0})}$$

If auxiliary variable \mathbf{p}'_j is accepted, update ω_{j0} to ω'_{j0} . Otherwise, set ω_{j0} to the current value.

S2. SENSITIVITY ANALYSIS FOR BOOST-ISING NORMALIZATION

Table S1 and S2 list five size factor estimation and three variance-stabilizing transformation (VST) methods for normalizing sequence count data, respectively. We conducted a sensitivity analysis to investigate how different normalization approaches affect the SV gene identification. We simulated ten replicated datasets following the data generating process described in the Simulation Study section. We include only the scenario with the medium zero-inflation setting (30% false zeros) and the two real spatial patterns (MOB II and BC). We assessed the model performance in terms of AUC.

The result is summarized in Figure S1. BOOST-Ising was robust to the four size factor-based normalization methods. We conducted ANOVA tests on all pairs of the four methods, and all p -values were greater than 0.05. The performance of BOOST-Ising based on the three VST approaches was similar but not satisfying.

S3. SENSITIVITY ANALYSIS FOR BOOST-ISING DICHOTOMIZATION

BOOST-Ising provides two clustering approaches, k -means and Gaussian mixture modeling (GMM) to dichotomize the relative expression levels for each gene. To evaluate the performance between the two choices, we conducted a sensitivity analysis. We simulated ten replicated datasets following the data generating process described in the Simulation Study section. We include only the scenario with the medium zero-inflation setting (30% false zeros) and the two real spatial patterns (MOB II and BC). We assessed the model performance in terms of AUC.

The result is summarized in Figure S2. BOOST-Ising was robust to the two binarization methods. We conducted pairwise t -tests, and p -value= 0.585 and 0.850 for MOB II and BC pattern, respectively.

S4. SENSITIVITY ANALYSIS FOR ISING MODEL HYPERPARAMETERS

We conducted a sensitivity analysis to investigate the sensitivity of the Ising model to the choice of σ_ω and σ_θ . We applied BOOST-Ising to each of the replicated dataset under the scenario with the low zero-inflation setting (10% false zeros) and MOB II pattern. We varied values of σ_θ from 1/4 to 2 and σ_ω from 1 to 100. We chose five values for each hyperparameter, resulting in 25 combinations. We assessed the model performance in terms of both AUC and MCC, where the latter was based on a Bayes factor threshold of 150.

The result is summarized in Figure S3, clearly indicating that BOOST-Ising was not sensitive to the choices of hyperparameters.

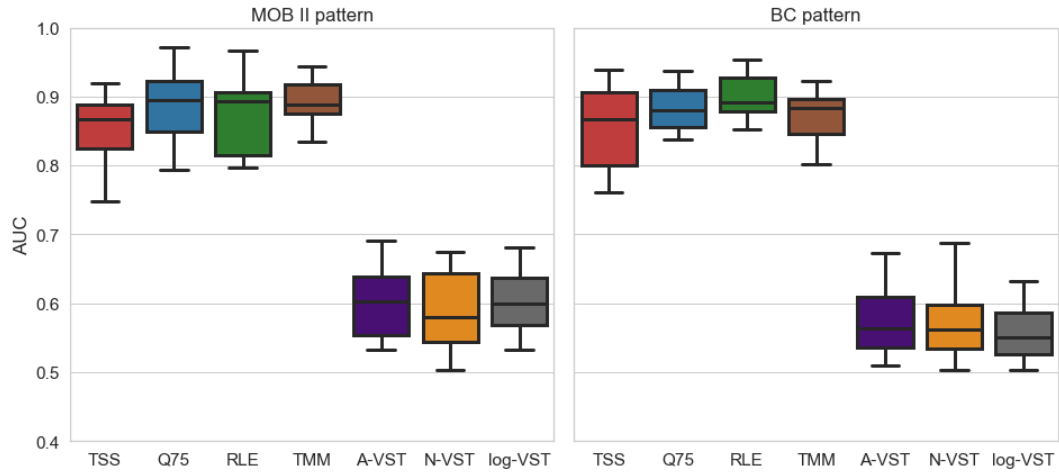


FIG. S1. Simulation study: The boxplots of AUCs achieved by different normalization methods in BOOST-Ising.

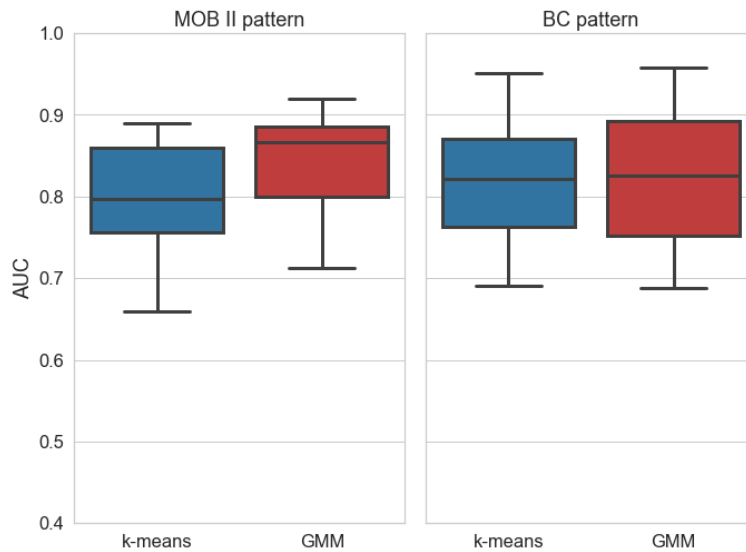


FIG. S2. Simulation study: The boxplots of AUCs achieved by different dichotomization methods in BOOST-Ising.

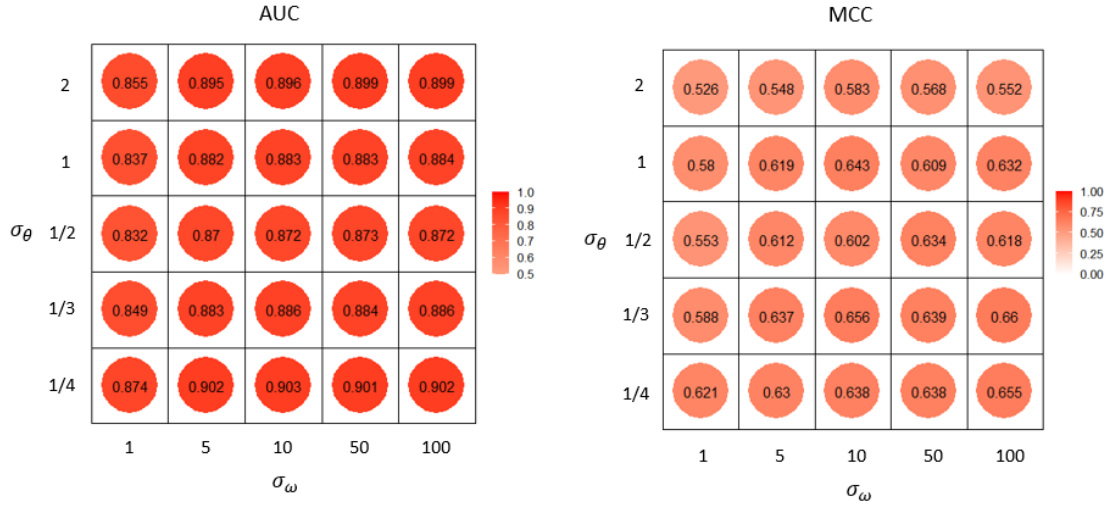


FIG. S3. Simulation study: The heatmaps of averaged AUCs and MCCs achieved by different Ising model hyperparameters σ_ω and σ_θ .

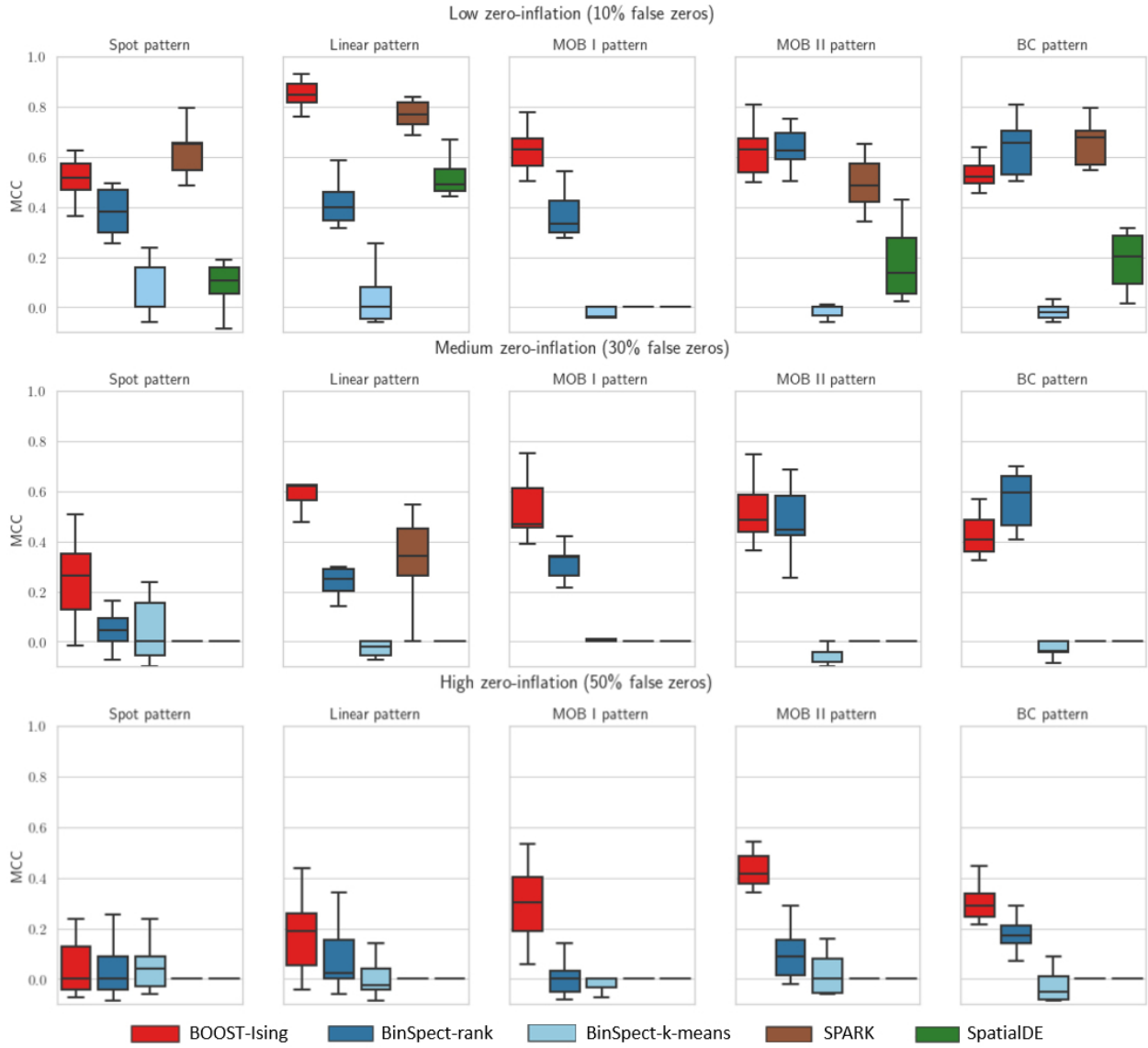


FIG. S4. Simulation study: The boxplots of MCCs achieved by BOOST-Ising, BinSpect, SPARK, and SpatialDE under different scenarios in terms of spatial pattern and zero-inflation setting.

TABLE S1. List of size factors used for normalizing sequence count data.

Abbreviation	Definition
none	$s_i \propto 1$
TSS	$s_i \propto Y_i$.
Q75 (Bullard et al., 2010)	$s_i \propto q_i^{0.75}$,
RLE (Anders and Huber, 2010)	$s_i \propto \text{median}_j \left\{ y_{ij} / \sqrt{\prod_{i'=1}^n y_{i'j}} \right\}$
TMM (Robinson and Oshlack, 2010)	$s_i \propto Y_i \cdot \exp \left(\frac{\sum_{j \in G^*} \psi_j(i,r) M_j(i,r)}{\sum_{j \in G^*} \psi_j(i,r)} \right)$

Note 1: q_i^x is defined as the x -th sample quantile of all the counts in sample i , i.e. there are xp features in sample i whose y_{ij} 's are less than q_i^x .

Note 2: The M -value $M_j(i, r) = \log(y_{ij}/Y_i)/\log(y_{rj}/Y_r)$ and A -value $A_j(i, r) = (\log y_{ij}/Y_i + \log y_{rj}/Y_r)/2$ are the ratio and average of log-scaled counts between sample i and the reference sample r , respectively. G^* denote a subset of genes whose M -values are not within the upper and lower 30% of all M -values and A -values are not within the upper and lower 5% of all A -values. The weight $\psi_j(i, r) = \frac{Y_i - y_{ij}}{y_{ij} Y_i} + \frac{Y_r - y_{rj}}{y_{rj} Y_r}$ is the inverse of the approximate asymptotic variances.

TABLE S2. List of variance-stabilizing transformations (VST) used for normalizing sequence count data.

Abbreviation	Definition
A-VST (Anscombe, 1948)	$g(y_{ij}, \phi) = \sinh^{-1} \sqrt{y_{ij}/\phi}$
N-VST (Love et al., 2014)	$g(y_{ij}, \phi) = \sinh^{-1} \sqrt{\frac{y_{ij} + 3/8}{\phi - 3/4}}$
log-VST (Anscombe, 1948; Svensson et al., 2018)	$g(y_{ij}, \phi) = \log(y_{ij} + \phi/2)$

Note 1: $\sinh^{-1}(y) = \log(y + \sqrt{1 + y^2})$.

Note 2: ϕ can be estimated via a non-linear model: $s_j^2 = \bar{y}_j + \bar{y}_j/\phi, j = 1, \dots, p$, where \bar{y}_j and s_j^2 denote the sample mean and variance of all the counts belonging to gene j , i.e. (y_{1j}, \dots, y_{nj}) .

TABLE S3. Simulation study: The averaged MCCs (standard deviations) achieved by BOOST-Ising, BinSpect, SPARK, and SpatialDE under different scenarios in terms of spatial pattern and zero-inflation setting.

	Low zero-inflation (10% false zeros)				
	Spot	Linear	MOB I	MOB II	BC
BOOST-Ising	0.519(0.071)	0.853 (0.054)	0.642 (0.103)	0.626(0.086)	0.531(0.108)
BinSpect-rank	0.341(0.176)	0.418(0.167)	0.333(0.172)	0.632 (0.080)	0.639(0.111)
BinSpect-km	0.061(0.117)	0.036(0.102)	0.041(0.158)	-0.019(0.035)	-0.021(0.032)
SPARK	0.624 (0.091)	0.768(0.053)	0.000(0.000)	0.488(0.116)	0.652 (0.083)
SpatialDE	0.128(0.136)	0.497(0.102)	0.000(0.000)	0.184(0.203)	0.276(0.197)
	Medium zero-inflation (30% false zeros)				
	Spot	Linear	MOB I	MOB II	BC
BOOST-Ising	0.237 (0.155)	0.604 (0.077)	0.568 (0.095)	0.501 (0.157)	0.398(0.071)
BinSpect-rank	0.067(0.111)	0.242(0.055)	0.306(0.096)	0.478(0.139)	0.567 (0.112)
BinSpect-km	0.049(0.126)	-0.004(0.076)	0.010(0.065)	-0.027(0.098)	-0.031(0.030)
SPARK	0.055(0.048)	0.342(0.164)	0.000(0.000)	0.065(0.113)	0.058(0.124)
SpatialDE	0.000(0.000)	0.000(0.000)	0.000(0.000)	0.000(0.000)	0.000(0.000)
	High zero-inflation (50% false zeros)				
	Spot	Linear	MOB I	MOB II	BC
BOOST-Ising	0.046 (0.108)	0.175 (0.158)	0.249 (0.166)	0.368 (0.107)	0.288 (0.139)
BinSpect-rank	0.046 (0.122)	0.075(0.141)	0.021(0.100)	0.095(0.097)	0.197(0.102)
BinSpect-km	0.046 (0.089)	0.008(0.108)	0.024(0.096)	0.018(0.078)	-0.044(0.063)
SPARK	0.000(0.000)	0.024(0.076)	0.000(0.000)	0.000(0.000)	0.048(0.101)
SpatialDE	0.000(0.000)	0.000(0.000)	0.000(0.000)	0.000(0.000)	0.000(0.000)

TABLE S4: Real data analysis on the MOB dataset: List of 60 SV genes that had an attraction pattern with a positive interaction parameter in the Ising model.

Gene	Bayes Factor	$BF \times 2 \times \ln(BF)$	Total Raw Count
Rc3h2	Inf	Inf	1174
Trib2	Inf	Inf	503
Med21	Inf	Inf	290
Nup210	Inf	Inf	163
Rsad1	Inf	Inf	94
Arap1	Inf	Inf	86
Zfp938	9999.000	18.420	190
Trim8	6665.667	17.609	809
Mrps18b	2856.143	15.914	192
Rbm15b	2499.000	15.647	151
Fam20c	2221.222	15.412	1603
Pdik1l	2221.222	15.412	143
Ccnh	951.381	13.716	1261
Ercc3	951.381	13.716	239

Vapa	868.565	13.534	4017
Dgke	713.286	13.140	393
Zfp248	713.286	13.140	109
Fen1	644.161	12.936	88
Amigo2	624.000	12.872	445
Mfap3	605.061	12.811	208
Katnal1	539.541	12.581	204
Tkt	525.316	12.528	518
Plekhm3	525.316	12.528	317
Ofd1	525.316	12.528	97
Mrps24	511.821	12.476	813
Wdr3	511.821	12.476	218
Pold3	499.000	12.425	227
Rcbtb1	486.805	12.376	552
Snx21	433.783	12.145	199
Fgf14	407.163	12.018	158
Nop58	376.358	11.861	248
Zfp9	337.983	11.646	144

Bbs5	326.869	11.579	249
Eif3c	284.714	11.303	1123
Chpf2	265.667	11.164	126
Ruvbl1	262.158	11.138	470
Zfp846	262.158	11.138	103
Umps	231.558	10.890	128
Pcnxl4	226.273	10.843	286
Cstf2	214.054	10.732	780
Pias2	209.526	10.690	920
Cog4	209.526	10.690	308
Dnalcl	205.186	10.648	616
Cnih3	205.186	10.648	287
Phyhipl	203.082	10.627	1488
Hnrnpf	203.082	10.627	819
Ncoa2	195.078	10.547	953
Atg13	195.078	10.547	728
X1700025G04Rik	187.679	10.469	794
X2310003H01Rik	184.185	10.432	94

Pin1	175.991	10.341	913
Nceh1	174.439	10.323	871
Lamtor5	172.913	10.306	356
Tmem42	171.414	10.288	157
Anks3	169.940	10.271	384
Crot	167.067	10.237	481
Tbc1d23	161.602	10.170	399
Armcx2	157.730	10.122	594
Nabp1	156.480	10.106	111
Rasgrp2	154.039	10.074	170
